



Article

Coaxial Wire Feeding-Friction Stir Additive Manufacturing

Mengmeng Liu D, Rui Wang D, Xiaohu Zhu D, Ximing Cheng and Songmo Li

Faculty of Ocean Engineering, Harbin Institute of Technology, Weihai 264200, China; 23s130222@stu.hit.edu.cn (M.L.); 22s130239@stu.hit.edu.cn (X.Z.); 24s130279@stu.hit.edu.cn (X.C.); 22s130246@stu.hit.edu.cn (S.L.)

* Correspondence: wang_rui@hit.edu.cn

Abstract

At present, most studies in the field of Wire-Friction Stir Additive Manufacturing (W-FSAM) adopt the side wire feeding method. However, the side wire feeding method has problems in that the wire feeding tube occupies working space and the tool is prone to clogging. To address this, this study proposes a Coaxial Wire Feeding-Friction Stir Additive Manufacturing (CWF-FSAM) method. The CWF-FSAM device adopts a structure where a fixed shaft is coaxially nested inside the stirring shaft, and the fixed shaft is machined with through-channels along the circumferential direction for wire feeding, which eliminates the limitation of the wire feeding tube. This study elaborates on the structure of the CWF-FSAM device, then uses 6061 aluminum alloy as the deposition material for additive manufacturing, and conducts characterization and analysis on the microstructure and mechanical properties of the deposited components. The results show that the interlayer bonding of the deposited components is dense without defects. The components exhibit uniform and fine equiaxed grains, with the average grain sizes of the top, middle, and bottom parts being 3.52 µm, 3.35 µm, and 4.07 µm, respectively. In terms of mechanical properties, the tensile strengths of the components along the building direction (BD) and longitudinal direction (LD) both reach 70% of that of the base material (BM) wire. The hardness ranges from 36 HV to 42 HV. In addition, closed-loop components were prepared by continuous counterclockwise deposition using the CWF-FSAM device. The tensile strengths of the overlapping area, straight section, and corner were 124.45 MPa, 125.88 MPa, and 126.95 MPa, respectively. The overall performance of the closed-loop components is uniform and stable, which indicates that the CWF-FSAM-deposited components have good mechanical property isotropy.

Keywords: wire-friction stir additive manufacturing; Aluminum alloy; mechanical properties



Academic Editor: Umberto Prisco

Received: 10 August 2025 Revised: 27 August 2025 Accepted: 28 August 2025 Published: 31 August 2025

Citation: Liu, M.; Wang, R.; Zhu, X.; Cheng, X.; Li, S. Coaxial Wire Feeding-Friction Stir Additive Manufacturing. *Crystals* **2025**, *15*, 784. https://doi.org/10.3390/cryst15090784

Copyright: © 2025 by the authors. Licensee MDPI, Basel, Switzerland. This article is an open access article distributed under the terms and conditions of the Creative Commons Attribution (CC BY) license (https://creativecommons.org/licenses/by/4.0/).

1. Introduction

The manufacturing methods of structural components can be divided into subtractive manufacturing [1] (such as turning and milling), equal material manufacturing [2] (such as forging, and casting), and additive manufacturing (AM) [3]. Subtractive manufacturing realizes component forming by removing materials, which has disadvantages such as material waste and difficulty in processing complex structures [4,5]. Equal material manufacturing changes the shape of materials through plastic deformation, and special molds need to be customized for complex structural components, resulting in long production cycles and large resource consumption [6,7]. In contrast, additive manufacturing is based on the principle of layer-by-layer material deposition, which has the advantages of high material utilization rate and strong design flexibility [8,9]. It can realize near-net

shape without complex process steps, and has gradually become a solution in the fields of lightweight structures and sustainable manufacturing [10–12]. Aluminum alloy, due to its low density and excellent formability, has become one of the most widely used metal materials in additive manufacturing [13,14].

Existing deposition technologies, such as laser [15] or electron beam [16] melting deposition technologies, use high-energy heat sources to melt materials and form deposition layers. However, this deposition method, which forms layers by melting materials and then cooling rapidly, has defects such as uneven microstructure and concentrated residual stress [17-19]. Differently from fusion deposition, friction-based solid-phase deposition technology deposits materials on the surface of the substrate without melting the materials [20-22]. Gandra et al. [23] stated that one of the earliest solid-phase deposition technologies is friction surface (FS) treatment. The working principle of FS technology is that under the action of pressure and the rotation of self-consuming metal rods, the metal rods undergo plastic deformation and deposit on the surface of the substrate [24]. Since then, solid-phase deposition technologies such as lateral friction surfacing (LFS) [25], friction stir welding (FSW) [26], friction stir additive manufacturing (FSAM) [27], additive friction stir deposition (AFSD) [28], hybrid metal extrusion and bonding technology [29], friction forged tubular additive manufacturing (FFTAM) [30], friction rolling additive manufacturing (FRAM) [31], and friction spiral extrusion additive manufacturing (FSEAM) [32] have emerged. Although existing solid-phase deposition technologies have made progress in controlling tissue defects compared with fusion deposition, most existing studies use plates, bars or powders as raw materials, and research on wire friction stir additive manufacturing is relatively scarce. In addition, deposition technologies such as FSAM, AFSD and FSEAM have the problem of discontinuous feeding, which easily leads to the interruption of the additive process and limits engineering applications [33].

To solve the problems of low design flexibility and discontinuous feeding in friction stir additive manufacturing, wire-friction stir additive manufacturing (W-FSAM) has achieved technological innovation through a continuous wire feeding mechanism. W-FSAM, proposed by Chen et al. [34] in 2023, adopts the side wire feeding method for friction stir additive manufacturing. Its process principle is that the spiral tool shears the wire, and the sheared material undergoes friction stir between the tool and the substrate or the previous deposition layer, causing severe plastic deformation of the material, and finally deposits on the additive surface. Chen et al. [35] prepared aluminum-copper alloy components with ultra-fine grains by W-FSAM technology, and the study concluded that precipitation strengthening is the main strengthening mechanism; Zhang et al. [36] prepared 6061 aluminum alloy components using a customized wire additive friction stir deposition (W-AFSD) device, analyzed the grain size of different parts of the components, and explored the deformation mechanism of the deposited components through in-situ tensile tests; Ton Bor et al. [37] proposed the friction spiral extrusion additive manufacturing (FSEAM) process, analyzed the microstructure and mechanical properties of the components, and specifically studied the influence of feed rate on forming quality. However, the side wire feeding method inevitably occupies working space due to the existence of the wire feed tube. In addition, Xie et al. [38] clearly pointed out that there is currently a problem of tool clogging in wire feeding-friction stir additive manufacturing.

In this regard, this study proposes Coaxial Wire Feeding-Friction Stir Additive Manufacturing (CWF-FSAM) technology. Compared with side wire feeding, the coaxial wire feeding method directly transports the wire into the spiral tool for shearing through the wire feeding channel processed along the circumferential direction of the fixed shaft. It not only eliminates the space limitation of the wire feed tube and improves the flexibility of the working space, but also the two through-channels designed along the circumferential

Crystals **2025**, 15, 784 3 of 13

direction of the fixed shaft can support the transportation of dissimilar wires, providing the possibility for material composite additive manufacturing. Since the research is still in the initial stage, only additive tests with a single material have been carried out in this study. This study introduces the CWF-FSAM device and systematically characterizes the microstructure and mechanical properties of the deposited components using 6061 aluminum alloy as the deposition material. In addition, the performance uniformity of the deposited components is explored by preparing closed-loop parts and testing the mechanical properties at the coincidence point and in different regions.

2. Materials and Methods

The device and process principle of Coaxial Wire Feeding-Friction Stir Additive Manufacturing (CWF - FSAM) are shown in Figure 1. Figure 1a is the physical view of the device, Figure 1b is the schematic diagram of the additive process, and Figure 1c is the schematic diagram of the overall structure of the device. In this study, a self-developed wire-friction stir additive manufacturing device is adopted, and its main components include a shell, a fixed shaft, a stirring shaft, a spiral tool, and a jacket. The fixed shaft and the stirring shaft adopt a coaxial nested structure. The fixed shaft is rigidly fixed to the device shell by bolts, and two through-channels are machined along the circumferential direction, which serve as special channels for wire feeding. The stirring shaft is connected to the spiral tool and drives the spiral tool to rotate at a high speed. The stirring system is composed of a fixed jacket and a rotatable spiral tool, both of which are made of H13 hot work die steel. The bottom diameter of the jacket is 24 mm, and it is fixedly connected to the shell. Two stirring pins are machined at the bottom of the spiral tool, with a length of 2 mm. The thickness of the deposited layer is 1.3 mm. During the deposition process, the stirring pins can pierce into the previous deposited layer, which facilitates more sufficient material mixing. Figure 1e is an enlarged view of part of the stirring system. The bottom surface of the fixed shaft is located on the upper surface of the cutting port of the spiral tool, ensuring that the wire is directly delivered to the cutting port of the tool. The wire spool serves as a continuous supply source of the wire and cooperates with the wire feeding mechanism to achieve stable wire feeding. Driven by the wire feeding mechanism, the wire is delivered to the cutting port of the spiral tool along the wire feeding channel of the fixed shaft, and then cut into fine particles by the high-speed rotating spiral tool. Subsequently, the particles fall onto the additive surface along the spiral trajectory, and undergo plastic deformation under the stirring and friction action of the spiral tool and the jacket, finally forming a deposited layer. Figure 1d,e are schematic diagrams of the Wire-Friction Stir Additive Manufacturing (W-FSAM) process. Before the start of deposition, the tool is moved to the preset position on the substrate in advance, as shown in Figure 1d. Then, the tool slowly descends to a position 1.3 mm above the substrate for rotational preheating, and the wire feeding is started at the same time. The preheating process promotes the material to undergo plastic deformation in advance, thereby improving the material fluidity during the deposition process. After preheating is complete, the formal deposition stage is entered. A reciprocating path is adopted for linear additive manufacturing, as shown in Figure 1e. After the deposition of the previous layer is complete, the tool is raised by 1.3 mm, and then moves in the opposite direction to complete the deposition of the next layer.

The material used in the experiment was commercially available 6061 aluminum alloy wire with a diameter of 1.6 mm. Additive deposition was carried out on a substrate with dimensions of 400 mm \times 400 mm \times 50 mm, and the substrate material was 6061 aluminum alloy. The chemical composition of the BM wire is shown in Table 1.

Crystals **2025**, 15, 784 4 of 13

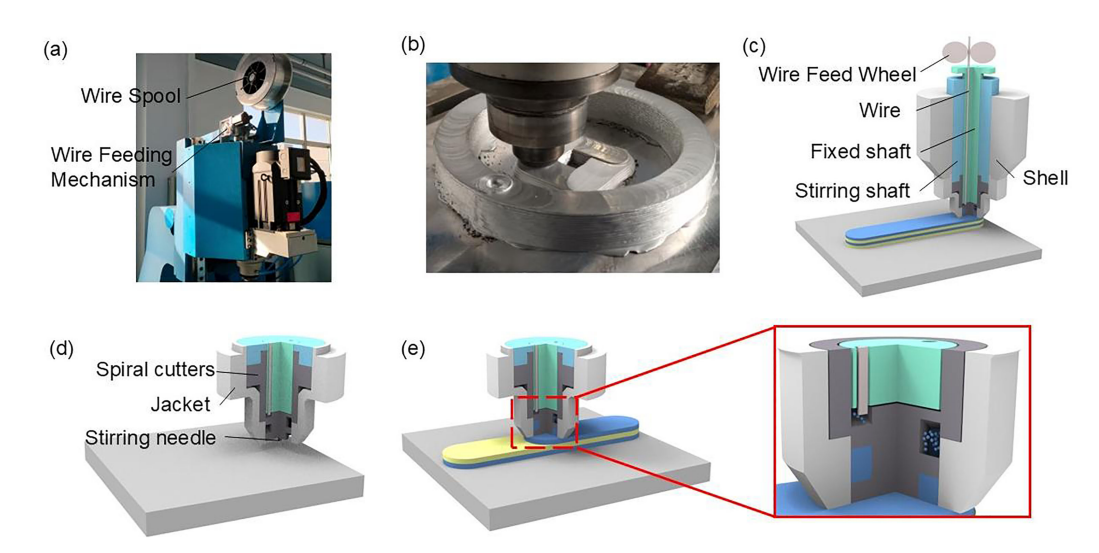


Figure 1. Schematic diagrams of the CWF-FSAM process: (a) diagram of the CWF-FSAM device; (b) schematic diagram of CWF-FSAM deposition; (c) schematic diagram of the CWF-FSAM structure; (d) schematic diagram of preheating; (e) schematic diagram of deposition with a reciprocating path.

Table 1. 6061 Aluminum alloy chemical composition table .

Element	Si	Fe	Cu	Mn	Mg	Zn	Ti	V	Al
6061	4.7	0.21	0.02	0.001	0.03	0.04	0.002	0.008	Bal

Rotational speed, travel speed, and wire feeding speed are the main influencing factors of the Wire-Friction Stir Additive Manufacturing (W-FSAM) process. The process parameters adopted in this study were a rotational speed of 700 rpm, a travel speed of 120 mm/min, a wire feeding speed of 1800 mm/min, and a layer thickness of 1.3 mm. A reciprocating deposition mode was used for the additive path. Finally, a linear deposited component with 27 layers was prepared, with a deposition length of 150 mm for each layer. The deposition result is shown in Figure 2a. Figure 2b shows the appearance morphology of the spiral tool after the completion of additive manufacturing. The tool is made of H13 hot work die steel, which has good wear resistance. It can be seen from Figure 2b that although the outer surface of the tool inevitably adheres to plastically deformed materials, no significant wear occurred.



Figure 2. Deposited components: (a) 27-layer deposited component; (b) appearance morphology of the spiral tool after deposition.

Samples were prepared from the deposited 27 layers by wire electrical discharge machining for microstructure and mechanical property analysis. The dimensions and positions of the samples are shown in Figure 3a. From left to right, they are, sequentially, longitudinal direction (LD) tensile samples, building direction (BD) tensile samples, X-ray diffraction (XRD) test samples, electron backscatter diffraction (EBSD) test samples, and hardness and ultra-depth-of-field test samples.

Crystals 2025, 15, 784 5 of 13

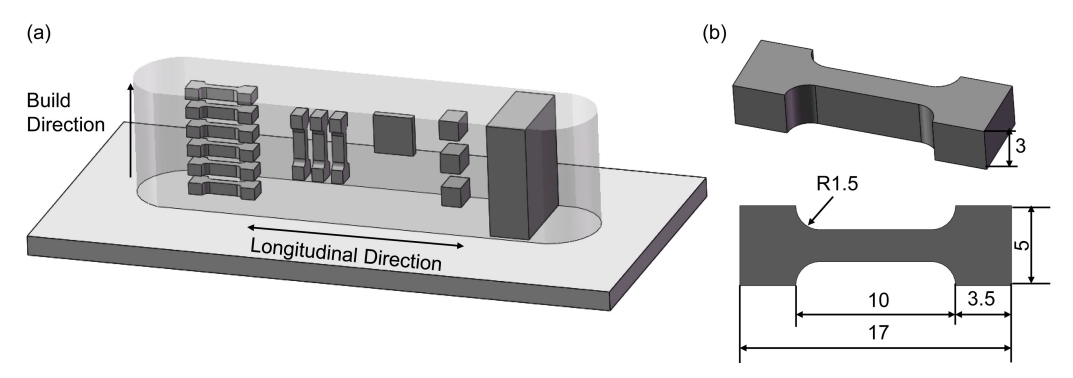


Figure 3. Cutting position: (a) cutting position and (b) tensile specimen size.

Tensile samples were cut from the top, middle, and bottom regions of the deposited component for longitudinal direction (LD) tensile tests, with two samples cut from each region. Three samples were cut along the building direction (BD), and the dimensions of the samples are shown in Figure 3b. The tensile tests were conducted using a Sans tensile testing machine, with the tensile speed set to 1 mm/min. A scanning electron microscope (SEM) was used to observe the tensile fracture morphology of the samples. Hardness samples were cut along the direction perpendicular to the longitudinal direction (LD), and the cut surface was used as the hardness testing surface. The experimental load was set to 100 g, the loading time was 10 s, and a hardness point was measured every 1 mm. X-ray diffraction (XRD) samples were ground sequentially with 80-mesh, 200-mesh, 500-mesh, 1000-mesh, 1500mesh, 2000-mesh, and 2500-mesh sandpapers, and then polished with a polishing agent. The samples were tested at room temperature using an X-ray diffractometer (Empyrean) produced by Malvern-PANalytical (Malvern, Worcestershire, UK). During the test, the working voltage was 45 kV, the accelerating current was 45 mA, the scanning range was 20–90°, and the scanning speed was 2°/min. For electron backscatter diffraction (EBSD) samples, the samples were first ground to 3000-mesh with sandpaper, and then embedded in PolyFast conductive resin for microstructure characterization. The embedded samples were gradually ground and polished with a 2.5 µm water-based diamond suspension, then finally calibrated with a 0.06 µm colloidal carbon dioxide solution, followed by vibratory polishing. The microstructure of the samples was characterized using a Tescan Miar4 with an Oxford Symmetry3 EBSD system, at a voltage of 20 keV and a step size of 0.11 μm. Ultra-depth-of-field samples were ground to 2000-mesh with sandpaper, polished to a mirror finish with a polishing agent, then etched with a hydrofluoric acid solution, and observed using a ultra-depth-of-field microscope(ZEISS, Jena, Germany).

3. Results

3.1. Macroscopic Morphology

Figure 4 shows the ultra-depth-of-field test results of the cross-section along the direction perpendicular to the longitudinal direction (LD). It can be seen from Figure 4a that the interlayer bonding of the Coaxial Wire Feeding-Friction Stir Additive Manufacturing (CWF-FSAM)-deposited component is dense, with no macroscopic defects such as cracks or pores. Figure 4b–d are partial magnified views of the left region. It can be observed from the figures that the interlayer boundary lines at both ends of the sample are clear and distributed horizontally, indicating that there is no interlayer material loss during the additive manufacturing process. The red dashed lines represent the material flow trajectory. The black dashed line regions represent the stir pin action zones. In this study, a reciprocating deposition path was adopted; under the action of the stir pin, the material mixing is more sufficient, which leads to the blurring of interlayer boundaries in the stir pin action zones, further confirming the denseness of interlayer bonding.

Crystals **2025**, 15, 784 6 of 13

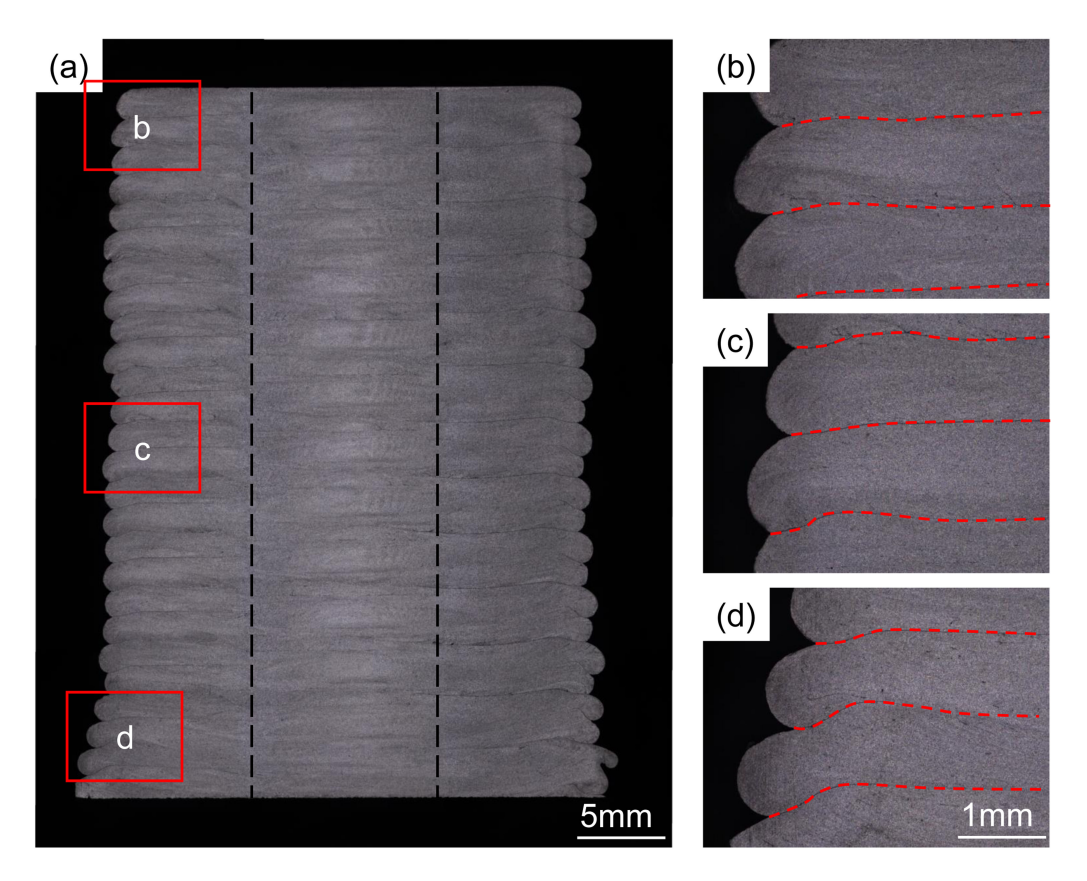


Figure 4. CWF-FSAM specimen cross-section: (a) macroscopic topography; (b) top magnification; (c) middle magnification; (d) bottom magnification.

3.2. Microstructure

Figure 5 shows the X-ray diffraction (XRD) results of the BM wire and the Coaxial Wire Feeding-Friction Stir Additive Manufacturing (CWF-FSAM)-deposited component. According to the XRD patterns, the BM wire and the CWF-FSAM-deposited component have the same phase composition, both containing two phases of Al and Si, with no new phases generated. In addition, compared with the BM wire, the diffraction peak intensities of the Al phase and Si phase in the CWF-FSAM-deposited component are both reduced. This phenomenon can be attributed to the severe plastic deformation and dynamic recrystallization during the additive manufacturing process, which leads to significant grain refinement.

To further investigate the microstructure of Coaxial Wire Feeding-Friction Stir Additive Manufacturing (CWF-FSAM)-deposited components, electron backscatter diffraction (EBSD) tests were conducted on the top, middle, and bottom regions of the deposited component to analyze the grain size, orientation distribution, and grain boundary characteristics of each region. The results are shown in Figure 6. Figure 6a,d,g are the inverse pole figures (IPF) of the top, middle, and bottom regions, respectively. According to the inverse pole figures, there is no obvious preferred orientation in any region, indicating that the deposited component has an isotropic microstructure. Figure 6b,e,h are the grain size maps of each region. The grain size in each region of the deposited component is uniform and fine, which is attributed to the severe plastic deformation of the material caused by shearing, friction stir, and extrusion during the additive manufacturing process, while the high temperature generated during the deposition process induces dynamic recrystallization. The average grain sizes of the top, middle, and bottom regions are 3.52 μ m, 3.35 μ m, and 4.07 μ m, respectively. Compared with the top and middle regions, the grain size of the bottom region is slightly larger. The reason is that the CWF-FSAM-deposited

Crystals **2025**, 15, 784 7 of 13

component is formed by layer-by-layer stacking from the bottom, and the bottom region is repeatedly subjected to the heat input from subsequent deposition layers, resulting in the growth of recrystallized grains. Figure 6c,f,i are the grain boundary misorientation angle distribution diagrams of each region, where a misorientation angle of 15° is used to distinguish high-angle grain boundaries (HAGBs) and low-angle grain boundaries (LAGBs). The proportions of high-angle grain boundaries in the top, middle, and bottom regions are 58.5%, 66.3%, and 70.5%, respectively. During the Wire-Friction Stir Additive Manufacturing process, the high-speed rotating tool interacts with the material through friction to generate a large amount of heat. At the same time, during the advancing process, the material undergoes plastic deformation under the extrusion friction of the tool and the stirring action of the stir pin, leading to an increase in dislocation density and strain energy accumulation. Driven by the interface energy, grain boundaries migrate continuously, and larger grains gradually engulf smaller grains, resulting in an increase in the misorientation angle between grains. Therefore, compared with the top and middle regions, the bottom region has larger grain size and the highest proportion of high-angle grain boundaries.

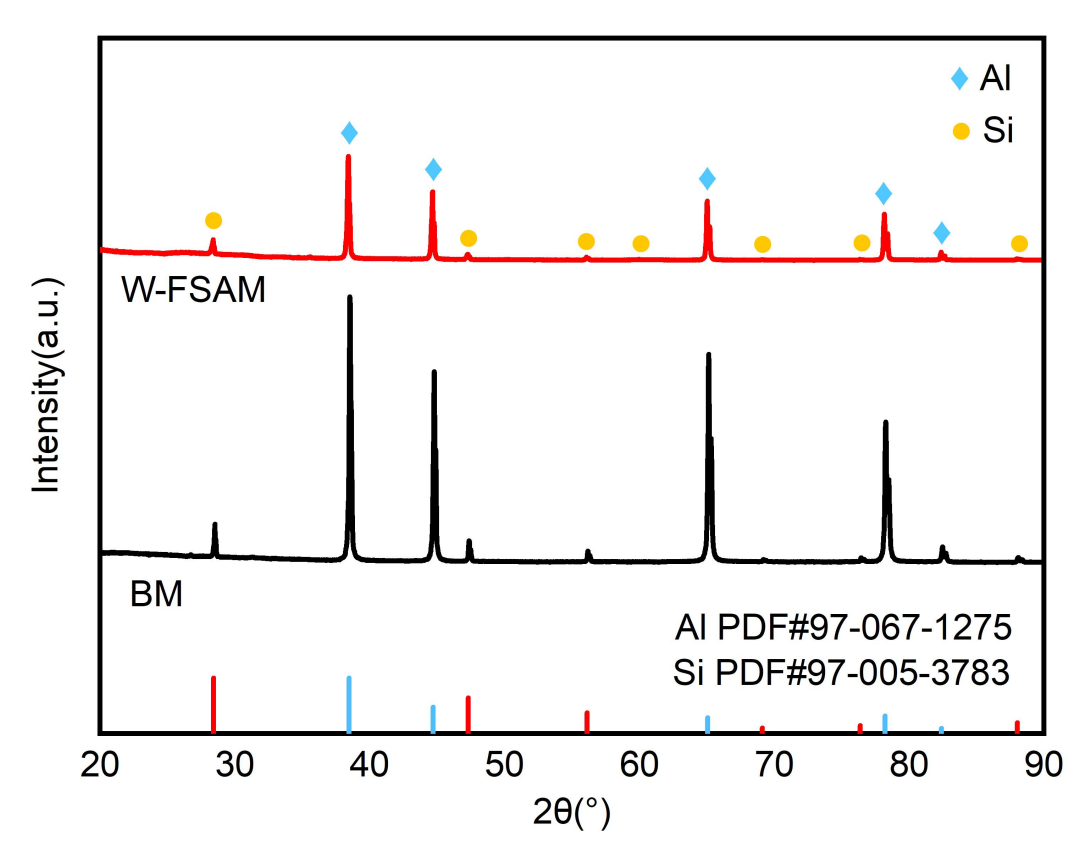


Figure 5. XRD image of a CWF-FSAM specimen.

3.3. Mechanical Properties

To evaluate the mechanical properties of the CWF-FSAM-deposited components, tensile tests were conducted on the BM wire and the top, middle, bottom regions, as well as along the BD direction of the CWF-FSAM-deposited components. The tensile test results are shown in Figure 7. The strengths of the deposited components along the LD and BD directions are both lower than that of the BM wire. This is because the high temperature during the deposition process causes dislocation rearrangement and a decrease in dislocation density, which ultimately results in a reduction in the strength of the deposited components. The tensile strengths along the BD direction, and of the top, middle, and bottom regions are 123.4 ± 0.27 MPa, 124.3 ± 1.29 MPa, 123.3 ± 2.59 MPa, and 126.4 ± 1.27 MPa, respectively. The strength differences among the regions are not

Crystals **2025**, 15, 784 8 of 13

significant, and all reach 70% of the strength of the BM wire, further confirming the uniformity of the mechanical properties of the components. In addition, compared with the BM wire, the elongation of the deposited components along the LD and BD directions is significantly improved, indicating that the deposited components have good plasticity.

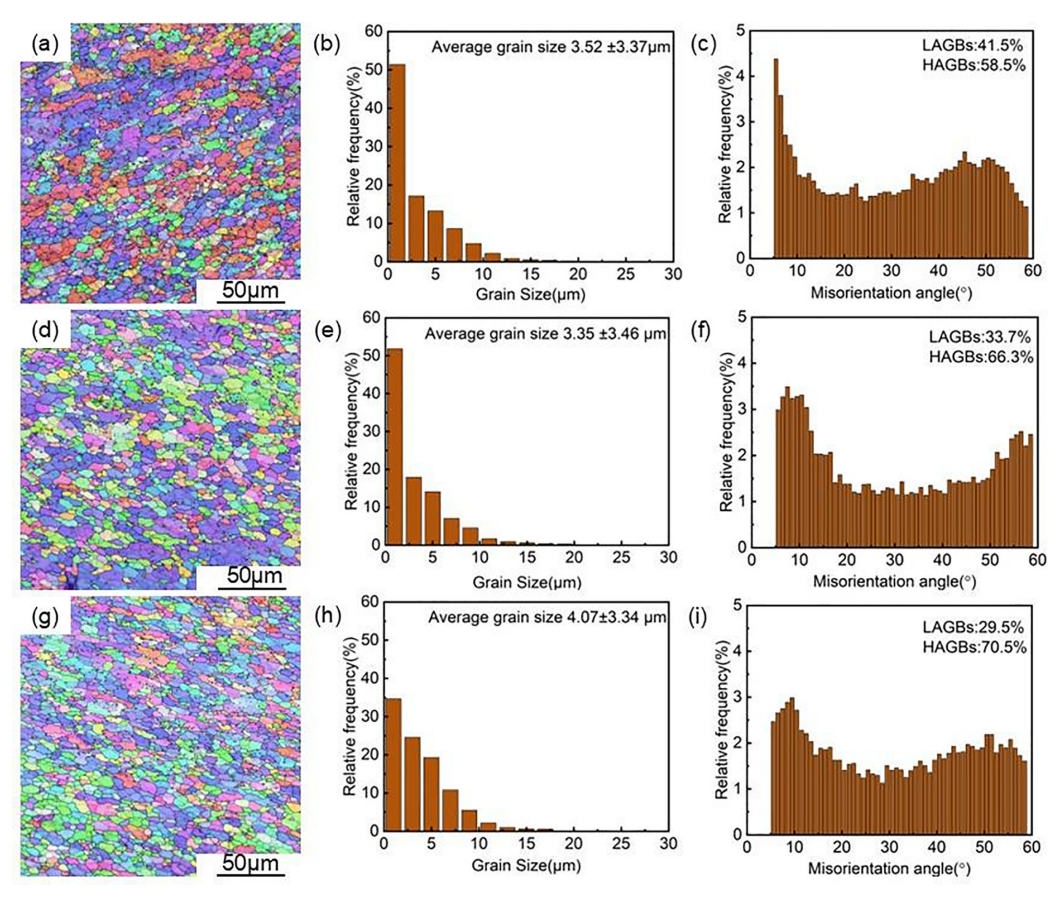


Figure 6. EBSD analysis: (a-c) top, (d-f) middle, and (g-i) bottom.

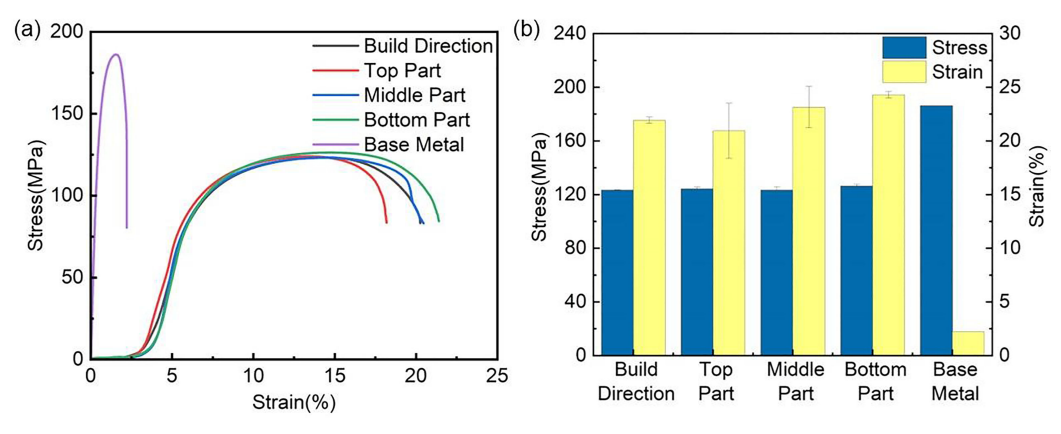


Figure 7. Tensile test analysis: (a) stress–strain curves and (b) comparison of tensile properties.

Figure 8a–d show the scanning electron microscope (SEM) morphologies of the fracture surfaces at different positions of the CWF-FSAM tensile-fractured samples, corresponding to the tensile fracture surfaces along the BD direction, and of the top, middle, and bottom regions, respectively. It can be seen from the results that the fracture surfaces at all positions exhibit equiaxed dimple characteristics, indicating that the deposited components undergo ductile fracture during the tensile process. Figure 8j shows the morphology of shallow dimples with a low dimple distribution density. Corresponding to the tensile data in Figure 7a, this indicates that the plasticity of the top sample is slightly worse than that of

other positions. Figure 8l shows the characteristics of deep dimples with a dense dimple distribution. Deep dimples usually mean that the material needs to overcome greater interfacial bonding force when subjected to stress, indicating that the bottom sample has higher strength and plasticity.

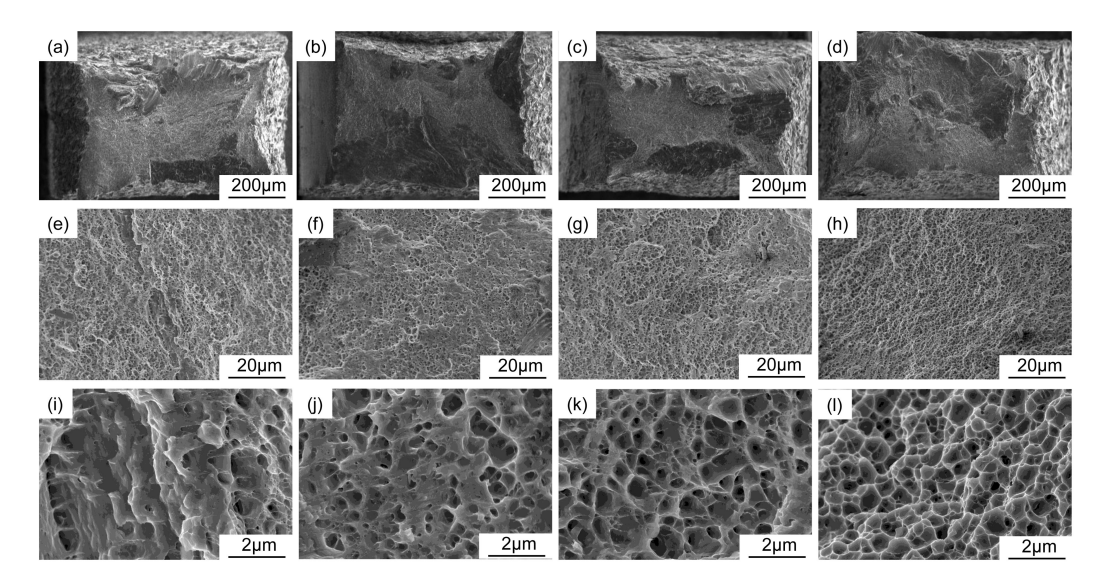


Figure 8. Topography of the tensile fracture: (a,e,i) build direction, (b,f,j) top, (c,g,k) middle, and (d,h,l) bottom.

Vickers hardness tests were conducted on the Coaxial Wire Feeding-Friction Stir Additive Manufacturing (CWF-FSAM)-deposited components. The hardness test points are shown in Figure 9a; along the BD direction from the top to the bottom of the component, a test point was set at every 1 mm interval. Figure 9b presents the hardness test results, from which it can be seen that the hardness of the component's top region is slightly higher than that of the middle and bottom regions. This is because the top region undergoes fewer thermal cycles during the deposition process and has smaller grain size; thus, the hardness of the top region of the sample is higher. The average hardness values of the three characteristic regions (Region 1, Region 2, and Region 3) are 38.78 ± 0.93 HV, 39.54 ± 0.99 HV, and 39.59 ± 1.49 HV, respectively. Along the BD direction, the hardness values fluctuate within the range of 36–42 HV overall, reaching 80% of the hardness of the wire used in the experiment (the hardness of the BM wire is 47.4 HV). In addition, there is no significant difference between the hardness data of different regions, indicating that the deposited component has good uniformity in hardness performance.

3.4. Tensile Properties of Closed-Loop Additive Components

Figure 10 shows the 6061 aluminum alloy closed-loop components fabricated by the CWF-FSAM technology. Both the circular ring component and the square component were formed by layer-by-layer stacking of the tool in the counterclockwise direction. Figure 10a shows the circular component with a diameter of 200 mm and 15 additive layers. Figure 10b shows the square component with a side length of 80 mm and 20 additive layers. During the deposition process of the closed-loop component, since the starting point and end point of the deposition path coincide, the overlapping region is prone to tool clogging due to redundant material accumulation, which in turn leads to the interruption of the additive process. To solve this problem, this study reduced material accumulation by increasing the lifting speed of the tool at the overlapping point; however, it should be noted that an excessively fast lifting speed may cause a decrease in the bonding denseness of the material, leading to a reduction in the strength of the overlapping region. Figure 10d shows

the linear deposited component fabricated when the tool lifting speed was relatively fast, and obvious forming defects at both ends of the component can be observed from the appearance morphology. This issue can be improved by reducing the lifting speed of the tool or setting a short pause when the tool is lifted. Sun et al. [39] also pointed out in their study that pausing for 0.5 s when lifting the tool can improve the bonding denseness of the material at both ends. Therefore, to prevent the strength reduction of the overlapping region caused by the increased tool lifting speed, it is very necessary to conduct tensile property tests on the overlapping region. Figure 10c is a schematic diagram of the sampling positions of the square component, and tensile property analysis was conducted on the overlapping region (NO. 1), the linear deposition section (NO. 2), and the corner (NO. 3).

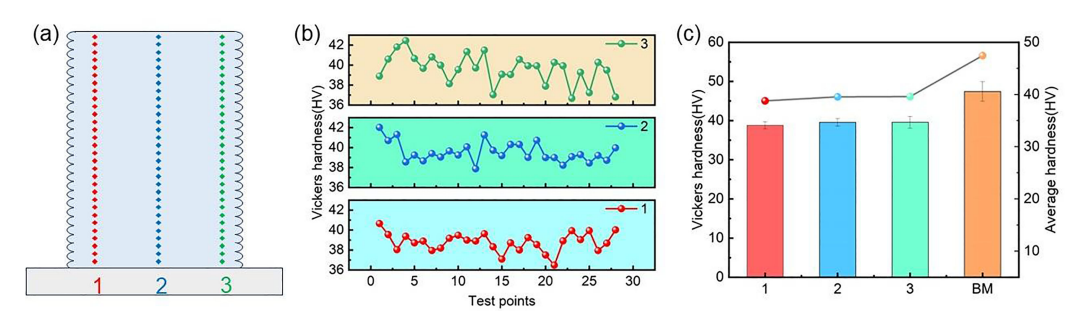


Figure 9. Hardness of CWF-FSAM-deposited component: (a) positions of hardness test points in Regions 1, 2, and 3; (b) hardness test results of Regions 1, 2, and 3; (c) average hardness of Regions 1, 2, 3, and BM wire.

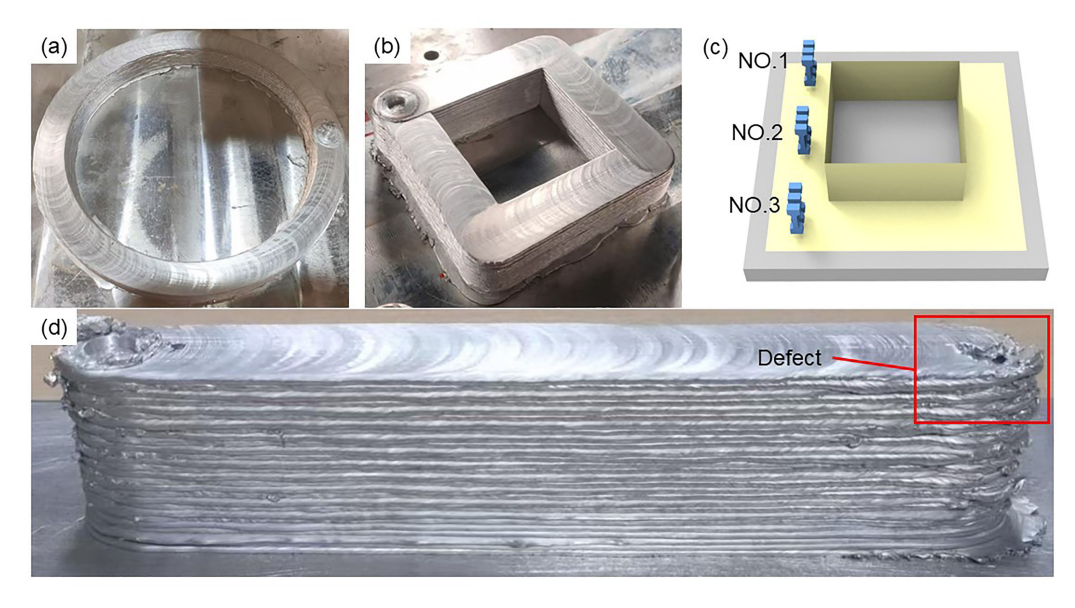


Figure 10. Closed-loop components: (a) circular ring component; (b) square component; (c) sampling positions for tensile testing of the square component; (d) deposited component with a relatively fast lifting speed.

Figure 11 shows the tensile test results of different regions of the square component. The tensile strengths of the overlapping point, linear section, and corner are 124.45 ± 1.67 MPa, 125.88 ± 0.43 MPa, and 126.95 ± 1.26 MPa, respectively, and the strength levels are essentially the same. The plasticity of the overlapping point is slightly lower than that of the linear section and the corner. This is because the lifting speed of the tool at the overlapping point is relatively fast, which causes the material to fail to undergo sufficient plastic flow, and ultimately results in a slight decrease in plasticity. In terms of overall performance, although the lifting speed of the tool at the overlapping region is increased, its tensile strength does not decrease significantly compared with that of the

linear section and the corner, indicating the consistency of the mechanical properties of the deposited component.

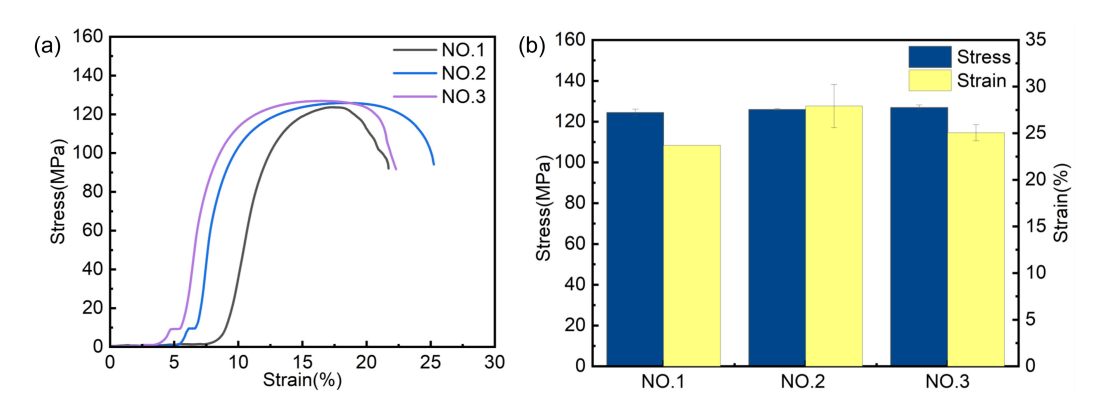


Figure 11. Square tensile results: (a) stress-strain curves and (b) comparison of tensile properties.

4. Conclusions

This study proposes a Coaxial Wire Feeding-Friction Stir Additive Manufacturing (CWF-FSAM) method, which eliminates the limitation of the side wire feeding tube on the working space in the existing W-FSAM technology, avoids the risk of tool clogging, and provides a new technical approach for the composite additive manufacturing of dissimilar wires. In this study, linear, circular, and square components were successfully deposited, and their microstructures and mechanical properties were investigated. The main conclusions are as follows:

- CWF-FSAM realizes top wire feeding by coaxially nesting a fixed shaft inside the stirring shaft and machining a through-type wire feeding channel along the circumferential direction of the fixed shaft. The components prepared based on CWF-FSAM have dense interlayer bonding and no obvious defects, which verifies the feasibility of the device.
- 2. Under the friction stir action of the stirring pin, the CWF-FSAM-deposited components obtain uniform and fine equiaxed grains. The average grain sizes of the top, middle, and bottom parts are $3.52~\mu m$, $3.35~\mu m$, and $4.07~\mu m$, respectively. The grain size distribution in each region is uniform, with no significant differences.
- 3. The strengths in the BD direction, top, middle, and bottom parts are 123.4 ± 0.27 MPa, 124.3 ± 1.29 MPa, 123.3 ± 2.59 MPa, and 126.4 ± 1.27 MPa, respectively, all reaching 70% of the wire strength. Compared with the wire, the plasticity of the CWF-FSAM structural components is significantly improved.
- 4. The average hardness values of the left, middle and right parts of the CWF-FSAM structural components are 38.78 ± 0.93 HV, 39.54 ± 0.99 HV, and 39.59 ± 1.49 HV, respectively, reaching 80% of the wire hardness. The hardness difference between different regions is not obvious, indicating that the components have good mechanical isotropy.
- 5. Closed-loop components were continuously prepared in the counterclockwise direction. The strengths of the square closed-loop component at the overlapping point, linear region, and corner are 124.45 ± 1.67 MPa, 125.88 ± 0.43 MPa, and 126.95 ± 1.26 MPa, respectively. The strength at the overlapping point does not decrease due to the increase in tool lifting speed, which further confirms the uniformity of the mechanical properties of the CWF-FSAM components.

Crystals 2025, 15, 784 12 of 13

Author Contributions: Conceptualization, M.L. and R.W.; methodology, M.L. and R.W.; validation, M.L.; formal analysis, X.Z.; investigation, X.Z.; resources, R.W.; data curation, M.L.; writing—original draft preparation, M.L.; writing—review and editing, M.L.; visualization, R.W.; supervision, R.W.; project administration, S.L. and X.C.; funding acquisition, S.L. All authors have read and agreed to the published version of the manuscript.

Funding: This work was supported by the "Equipment Pre-research Key Laboratory Foundation of China" (No. 61420052022KJW02) and the "Aeronautical Science Foundation of China" (No. 20230011077002).

Data Availability Statement: The original contributions presented in the study are included in the article; further inquiries can be directed to the corresponding author.

Conflicts of Interest: The authors declare no conflicts of interest.

References

- 1. Jingbin, Z.; Lei, G.; Weiqiang, Z.; Xifeng, C. Research progress on friction stir additive manufacturing technology. *Therm. Work. Technol.* **2024**, *53*, 30–38. [CrossRef]
- 2. Wang, H.; Li, Y.; Yang, B.; Wang, J.; Wang, Z.; Li, Y. Unveiling the mechanism of texture evolution in AZ31B Mg alloy during additive friction stir deposition. *J. Alloys Compd.* **2025**, *1011*, 178404. [CrossRef]
- 3. Lei, S.; Yang, L.; Yichen, X.; Chuansong, W.; Huijie, L. Research progress of metal solid phase additive manufacturing based on friction stir. *J. Mater. Eng.* **2022**, *50*, 1–14. [CrossRef]
- 4. Lei, W.; Bingheng, L. Research on additive manufacturing technology and industrial development in our country. *Strateg. Study CAE* **2022**, 24, 202–211. [CrossRef]
- 5. Lu, I.K.; Reynolds, A.P. Innovative friction stir additive manufacturing of cast 2050 Al–Cu–Li aluminum alloy. *Prog. Addit. Manuf.* **2021**, *6*, 471–477. [CrossRef]
- 6. Hongyu, D.; Shuting, W.; Kang, Y.; Chaoping, S.; Fan, W.; Chao, C.; Yanbing, T.; Zhiyong, J. Research progress on domestic and foreign standards for additive manufacturing. *Prog. Mater. China* **2020**, *39*, 955–961. [CrossRef]
- 7. Yao, J.; Dai, G.; Guo, Y.; Li, W.; Sun, Z.; Shen, Z.; Luo, K.; Chang, H.; Zhou, L. Microstructure and properties of solid-state additive manufactured Mg–10Li–3Al–3Zn magnesium alloy. *J. Mater. Res. Technol.* **2023**, 25, 4820–4832. [CrossRef]
- 8. Li, H.; Wang, C.; Zhang, H.; Zhang, J.; He, P.; Shao, M.; Zhu, X.; Fu, Y. Research progress of friction stir additive manufacturing technology. *Acta Metall. Sin.* **2022**, *59*, 106–124. [CrossRef]
- 9. Di Pompeo, V.; Santecchia, E.; Santoni, A.; Sleem, K.; Cabibbo, M.; Spigarelli, S. Microstructure and defect analysis of 17-4PH stainless steel fabricated by the Bound Metal Deposition additive manufacturing technology. *Crystals* 2023, 13, 1312. [CrossRef]
- 10. Shao, J.; Samaei, A.; Xue, T.; Xie, X.; Guo, S.; Cao, J.; MacDonald, E.; Gan, Z. Additive friction stir deposition of metallic materials: Process, structure and properties. *Mater. Des.* **2023**, 234, 112356. [CrossRef]
- 11. Agrawal, P.; Haridas, R.S.; Yadav, S.; Thapliyal, S.; Gaddam, S.; Verma, R.; Mishra, R.S. Processing-structure-property correlation in additive friction stir deposited Ti-6Al-4V alloy from recycled metal chips. *Addit. Manuf.* **2021**, 47, 102259. [CrossRef]
- 12. Kar, A.; Kumar, S.; Kailas, S.V. Developing multi-layered 3D printed homogenized structure using solid state deposition method. *Mater. Charact.* **2023**, 199, 112770. [CrossRef]
- 13. Chen, L.; Li, Y.; Lu, L.; Yang, Z.; Ren, X.; Zhang, X. The effect of heat treatment on the microstructure and mechanical properties of multilayer AA6061 alloy fabricated by additive friction stir deposition. *Mater. Today Commun.* **2024**, *38*, 108078. [CrossRef]
- 14. Zhang, M.; Jiang, T.; Sun, Z.; Feng, S.; Ma, L.; Wang, W.; Su, Y.; Xu, Y.; Li, W. Screw-fed powder-based additive friction stir deposition: A study on pure aluminum. *J. Mater. Process. Technol.* **2025**, 337, 118730. [CrossRef]
- 15. Gong, J.; Wei, K.; Liu, M.; Song, W.; Li, X.; Zeng, X. Microstructure and mechanical properties of AlSi10Mg alloy built by laser powder bed fusion/direct energy deposition hybrid laser additive manufacturing. *Addit. Manuf.* **2022**, *59*, 103160. 10.1016/j.addma.2022.103160. [CrossRef]
- 16. Markl, M.; Tinat, M.R.A.; Berger, T.; Westrich, Y.; Renner, J.; Koerner, C. In-situ electron beam characterization for electron beam powder bed fusion. *Addit. Manuf.* **2024**, *96*, 104567. [CrossRef]
- 17. Karmakar, S.; Swarnkar, R.; Pal, S.K. Effect of multi-layer deposition in solid-state friction stir surfacing-based additive manufacturing for fabrication of large-scale metal product. *J. Mater. Process. Technol.* **2023**, 320, 118107. [CrossRef]
- 18. Liu, H.; Xu, T.; Li, J.; Xie, R.; Chen, Y.; Huang, N.; Chen, S.; Xiao, J.; Chen, S. Solid-state friction rolling repair technology for various forms of defects through multi-layer multi-pass deposition. *J. Manuf. Processes* **2024**, *127*, 62–76. [CrossRef]
- Zhang, Y.; Guan, X.; Wang, L.; Wang, X.; Zhan, X. The microstructure diversity in different areas of the ring-route Al 6061-T6 additive zone by friction stir additive manufacturing. *Int. J. Adv. Manuf. Technol.* 2023, 128, 4857–4871. 10.1007/s00170-023-11882-4. [CrossRef]

20. Korgancı, M.; Bozkurt, Y. Recent developments in additive friction stir deposition (AFSD). *J. Mater. Res. Technol.* **2024**, 30, 4572–4583. [CrossRef]

- 21. Gao, H.; Li, H. Friction additive manufacturing technology: A state-of-the-art survey. *Adv. Mech. Eng* **2021**, *13*, 16878140211034431. [CrossRef]
- 22. Hang, Z.Y.; Hahn, G.D. Potential and challenges for large-scale near-net-shaping of 7xxx aerospace grade aluminum via additive friction stir deposition. *Mater. Lett.* **2023**, *19*, 100217. [CrossRef]
- 23. Gandra, J.; Krohn, H.; Miranda, R.; Vilaça, P.; Quintino, L.; dos Santos, J.F. Friction surfacing—A review. *J. Mater. Process. Technol.* **2014**, 214, 1062–1093. [CrossRef]
- 24. Li, H.; Cao, B.; Gao, H.; Wang, B.; Zhou, J. Multilayer friction surfacing of AA6061 aluminum alloy on 316L steel plate. *Proc. Inst. Mech. Eng. Part L J. Mater. Des. Appl.* **2023**, 237, 727–736. [CrossRef]
- 25. Seidi, E.; Miller, S.F. Thermo-mechanical finite element analysis of the solid-state metal deposition via lateral friction surfacing. CIRP J. Manuf. Sci. Technol. 2024, 50, 127–139. [CrossRef]
- 26. Hu, X.; Luo, Z.; Liu, S.; Ren, Y.; Long, W. Effect of Stirring Needle Length on the Microstructures and Properties of A380/6061 Dissimilar Aluminium Alloy FSW Joints. *Materials* **2025**, *18*, 1621. [CrossRef]
- 27. Li, Y.; He, C.; Wei, J.; Zhang, Z.; Tian, N.; Qin, G.; Zhao, X. Restirring and reheating effects on microstructural evolution of Al–Zn–Mg–Cu alloy during underwater friction stir additive manufacturing. *Materials* **2022**, *15*, 3804. [CrossRef]
- 28. Chen, G.; Wu, K.; Wang, Y.; Sun, Y.; Wang, X.; Zhu, Z.; Hu, F. Quantitative study on the correlation between microstructure and mechanical properties of additive friction stir deposited 6061-T6 Al-Mg-Si alloy. *J. Mater. Res. Technol.* **2023**, 25, 6725–6736. [CrossRef]
- 29. Blindheim, J.; Welo, T.; Steinert, M. First demonstration of a new additive manufacturing process based on metal extrusion and solid-state bonding. *Int. J. Adv. Manuf. Technol.* **2019**, *105*, 2523–2530. [CrossRef]
- 30. Derazkola, H.A.; Khodabakhshi, F.; Gerlich, A. Friction-forging tubular additive manufacturing (FFTAM): A new route of solid-state layer-upon-layer metal deposition. *J. Mater. Res. Technol.* **2020**, *9*, 15273–15285. [CrossRef]
- 31. Xie, R.; Shi, Y.; Liu, H.; Chen, S. A novel friction and rolling based solid-state additive manufacturing method: Microstructure and mechanical properties evaluation. *Mater. Today Commun.* **2021**, 29, 103005. [CrossRef]
- 32. Rezaeinejad, S.; Strik, D.; Visser, R.; Bor, T.; Luckabauer, M.; Akkerman, R. Solid-state additive manufacturing of AA6060 employing friction screw extrusion additive manufacturing. *J. Miner. Met. Mater. Soc.* **2023**, *75*, 4199–4211. [CrossRef]
- 33. Wang, J.; Xie, Y.; Meng, X.; Zhao, Y.; Sun, S.; Li, J.; Chen, J.; Chen, H.; Ma, X.; Wang, N.; et al. Wire-based friction stir additive manufacturing towards isotropic high-strength-ductility Al-Mg alloys. *Virtual Phys. Prototyp.* **2024**, *19*, e2417369. [CrossRef]
- 34. Chen, H.; Meng, X.; Chen, J.; Xie, Y.; Wang, J.; Sun, S.; Zhao, Y.; Li, J.; Wan, L.; Huang, Y. Wire-based friction stir additive manufacturing. *Addit. Manuf.* 2023, 70, 103557. [CrossRef]
- 35. Chen, H.; Zou, N.; Xie, Y.; Meng, X.; Ma, X.; Wang, N.; Huang, Y. Wire-based friction stir additive manufacturing of AlCu alloy with forging mechanical properties. *J. Manuf. Processes* **2025**, *133*, 354–366. [CrossRef]
- 36. Zhang, M.; Jiang, T.; Feng, X.; Xie, Y.; Su, Y.; Sun, Z.; Wang, W.; Xu, Y.; Li, W. Investigation on in-situ tensile behaviors of 6061 aluminum alloy fabricated by wire additive friction stir deposition. *J. Alloys Compd.* **2024**, *1008*, 176780. [CrossRef]
- 37. Bor, T.; De Leede, M.; Deunk, F.; Lind, J.; Lievestro, W.; Smit, H.J.; Ariës, R.; Dolas, V.; Helthuis, N.; Luckabauer, M.; et al. Friction screw extrusion additive manufacturing of an Al-Mg-Si alloy. *Addit. Manuf.* **2023**, 72, 103621. [CrossRef]
- 38. Xie, Y.; Huang, Y.; Meng, X.; Zhang, R. A Rotary Chopping Type Friction Stir Additive Manufacturing Device and Method, China Patent CN115647560B. 5 September 2023.
- 39. Sun, X.; Xie, Y.; Meng, X.; Zhang, Z.; Tian, H.; Dong, W.; Dong, J.; Ma, X.; Wang, N.; Huang, Y. Wire-based friction stir additive manufacturing of AZ31B magnesium alloy: Precipitate behavior and mechanical properties. *J. Magnes. Alloy* **2025**. [CrossRef]

Disclaimer/Publisher's Note: The statements, opinions and data contained in all publications are solely those of the individual author(s) and contributor(s) and not of MDPI and/or the editor(s). MDPI and/or the editor(s) disclaim responsibility for any injury to people or property resulting from any ideas, methods, instructions or products referred to in the content.